This article was downloaded by: [University of Otago]
On: 22 December 2014, At: 21:32
Publisher: Taylor & Francis
Informa Ltd Registered in England and Wales Registered Number: 1072954 Registered office: Mortimer House, 37-41 Mortimer Street, London W1T 3JH, UK

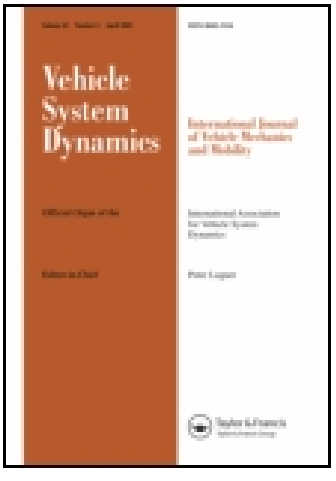

CrossMark
Click for updates

Vehicle System Dynamics: International Journal of Vehicle Mechanics and Mobility
Publication details, including instructions for authors and subscription information:
http://www.tandfonline.com/loi/nvsd20

Investigation of a passenger car's dynamic response due to a flywheel-based kinetic energy recovery system

Günter Bischof[a], Karl Reisinger[a], Thomas Singraber[a] & Andreas Summer[a]
[a] Institute of Automotive Engineering, FH Joanneum University of Applied Sciences, Graz, Austria
Published online: 13 Jan 2014.

To cite this article: Günter Bischof, Karl Reisinger, Thomas Singraber & Andreas Summer (2014) Investigation of a passenger car's dynamic response due to a flywheel-based kinetic energy recovery system, Vehicle System Dynamics: International Journal of Vehicle Mechanics and Mobility, 52:2, 201-217, DOI: 10.1080/00423114.2013.869609

To link to this article: http://dx.doi.org/10.1080/00423114.2013.869609

PLEASE SCROLL DOWN FOR ARTICLE

Taylor & Francis makes every effort to ensure the accuracy of all the information (the "Content") contained in the publications on our platform. However, Taylor & Francis, our agents, and our licensors make no representations or warranties whatsoever as to the accuracy, completeness, or suitability for any purpose of the Content. Any opinions and views expressed in this publication are the opinions and views of the authors, and are not the views of or endorsed by Taylor & Francis. The accuracy of the Content should not be relied upon and should be independently verified with primary sources of information. Taylor and Francis shall not be liable for any losses, actions, claims, proceedings, demands, costs, expenses, damages, and other liabilities whatsoever or howsoever caused arising directly or indirectly in connection with, in relation to or arising out of the use of the Content.

This article may be used for research, teaching, and private study purposes. Any substantial or systematic reproduction, redistribution, reselling, loan, sub-licensing, systematic supply, or distribution in any form to anyone is expressly forbidden. Terms &

Conditions of access and use can be found at http://www.tandfonline.com/page/terms-and-conditions

Downloaded by [University of Otago] at 21:32 22 December 2014

Vehicle System Dynamics, 2014
Vol. 52, No. 2, 201–217, http://dx.doi.org/10.1080/00423114.2013.869609

Taylor & Francis
Taylor & Francis Group

Investigation of a passenger car's dynamic response due to a flywheel-based kinetic energy recovery system

Günter Bischof*, Karl Reisinger, Thomas Singraber and Andreas Summer

Institute of Automotive Engineering, FH Joanneum University of Applied Sciences, Graz, Austria

(*Received 16 July 2013; accepted 21 November 2013*)

With the advent of flywheel-based kinetic energy recovery systems in automotive applications new safety issues arise as a consequence of the flywheel's high rotational speed. While the special structural safety requirements of the components are well discussed in the literature, there is still little research on the influence of gyroscopic effects on vehicle dynamics. The aim of this paper is to investigate the influence of a typical high-speed flywheel on the driving dynamics of an average passenger car. To this end the equations of motion of a gyroscope are derived, which relate the vehicle's roll, pitch and yaw rate with the transverse torque acting on the flywheel. These equations are implemented in a commercial vehicle dynamics simulation program in order to determine the reaction torques acting on the vehicle within a representative range of driving situations. Numerical simulations indicate that the gyroscopic effect can be considered insignificant in standard driving situations.

Keywords: vehicle dynamics; kinetic energy recovery system; flywheel; gyroscopic torque

Downloaded by [University of Otago] at 21:32 22 December 2014

1. Introduction

In recent years, the integration of kinetic energy recovery systems (KERS) in automotive applications has become a topic of increasing interest due to the need for improved fuel efficiency and reduced emissions. Such systems recover, store and reapply vehicle kinetic energy – energy that would otherwise have been wasted under braking. Electrical hybrid systems utilise a chemical battery or an ultracapacitor as the storage medium and electric motor/generator systems as the energy transfer and control media. In contrast, mechanical hybrid systems utilise a flywheel as the energy storage device and a variable transmission to control and transfer the energy to and from the driveline.

Electrical energy storage systems, on the one hand, have a high specific energy density, compactness and operational simplicity. On the other hand, they are lacking in recharge efficiency and suffer from transmission losses associated with energy conversion from mechanical energy to electrical energy and vice versa. Flywheels have excellent recharge efficiencies and virtually unlimited cycle lives. When they are coupled with a mechanical transmission the conversion losses are eliminated as the mechanical braking energy is transmitted and stored in the same form. Furthermore, they operate over a wider temperature range than electrical systems.

*Corresponding author. Email: guenter.bischof@fh-joanneum.at

© 2014 Taylor & Francis

Downloaded by [University of Otago] at 21:32 22 December 2014

The idea of coupling a flywheel to a motor/generator to emulate a battery for use in electric vehicles is about 60 years old. It dates back to the *Gyrobus*, a city bus developed by Oerlikon in Switzerland that ran on electric power generated by a spinning flywheel.[1] Although technically successful, the services were not commercially viable and ended in 1960.

In the 1980s, the General Motors Research Laboratories investigated the performance of an engine-flywheel hybrid powertrain in terms of its ability to improve the fuel economy of a compact car. The margin of improvement was judged insufficient to justify such a complex drivetrain and, therefore, a prototype system was not built.[2]

Most significant for the re-emergence of flywheel-driven KERS was the Fédération Internationale de l'Automobile's (FIA) decision to authorise the use of hybrid drivetrains for the 2009 Formula 1 racing season, with the clear intent of directing technical developments in motorsport to advance fuel efficiency technologies in mainstream vehicles. The specification of the hybrid systems has been kept to a minimum, with a focus on safety, only a limit on both the power rating of the hybrid system at 60 kW and the quantity of energy transfer per lap at 400 kJ has been specified.

After having evaluated all the potential hybrid system architectures from the motor/generator system with chemical battery to the pneumatic or hydraulic high pressure storage systems, *Williams Hybrid Power Limited*, *Flybrid Systems LLP* and *Ricardo UK Ltd*, all in the UK, developed flywheel units for use in Formula 1 as well as for mainstream automotive applications.[3]

In the *Flybrid Systems* solution, which is an all-mechanical flywheel system implementation, the energy storage is performed by a high-speed carbon filament flywheel enclosed in an evacuated housing; for the energy transfer a *Torotrak* full-toroidal traction drive continuously variable transmission (CVT) unit is employed.[4]

As a result of this development, hybrid drivetrain systems are becoming increasingly prevalent in automotive and commercial vehicle applications. Original equipment manufacturers from all over the world are looking to integrate KERS to improve fuel economy and reduce green house gas emissions. Flywheel-based KERSs have about twice the efficiency of battery-based hybrids and may improve the vehicle fuel economy by more than 30% [5] over driving cycles characterised by frequent engine starts and stops. As an additional benefit the KERS can provide an extra torque increasing the total torque available to accelerate the car, if required.[5–11]

Contemporary flywheel-based energy recovery systems rely on advanced high-strength materials, as flywheels usually operate at rotational speeds exceeding 60,000 rpm (the maximum angular velocity of the *Flybrid Systems* KERS is 64,500 rpm).[4] The flywheel thus exceeds the speed of any other rotating part of a car by an order of magnitude, which might account for noticeable gyroscopic effects in a moving vehicle.

Gyroscopic forces come into play whenever the vehicle departs from a straight-line course, as in cornering or turning. These effects can be minimised by vertically orienting the axis of rotation. The gyroscopic forces induced by body roll during cornering or by pitching upward or downward due to gear changes, bumps or road grades, however, cannot be compensated by such a preferred installation position. Since these forces are expected to be of a similar order of magnitude as the forces acting on the moving vehicle, they could have a detrimental influence on the vehicle's handling characteristics. This can be remedied by mounting the flywheel in a gimballed system, which allows the rotor to retain its original orientation without affecting the vehicle. Such a free-motion gimbal mounting, however, needs more installation space and results in an increased design complexity to communicate power into and out of the flywheel. By limiting the gimbal excursions to typical pitch and roll motions of a car, the space usage can be reduced, but additional shock absorbers have to be implemented to cushion sudden rapid motions. An alternative solution is to operate two flywheel modules

in pairs – one spinning clockwise, the other counter-clockwise. When both flywheels are maintained at the same speed the gyroscopic forces are almost balanced.

On the other hand, the gyroscopic torques produced by the flywheel could be utilised to stabilise a vehicle so as to keep it from rolling over. In a recent investigation,[12] the use of a flywheel-based KERS as an active gyroscopic stabilisation for an articulated lorry is proposed. In standard situations, the flywheel is supported by a double gimbal to avoid gyroscopic effects on the vehicle. When the lateral acceleration and the roll angle exceed a predefined safety limit, the external gimbal is constrained in such a way that the counter-torque prevents the rollover of the vehicle.

In this work, the influence of a rigidly mounted flywheel-based KERS on the driving dynamics of a typical passenger car is investigated. By neglecting any elasticity of the flywheel mounting, a strong coupling with the vehicle is established. The effect of the gyroscopic torque on the vehicle's road behaviour is simulated and discussed for some selected driving manoeuvres.

Downloaded by [University of Otago] at 21:32 22 December 2014

2. Derivation of the gyroscopic torques

To study the effects of the vehicle's motion on the flywheel, and its reactive gyroscopic forces exerted back on the vehicle, we seek an expression describing the torques that occur between the flywheel and its suspension. Similar problems have been studied extensively over the past couple of decades by aeronautics and spaceflight engineers in the context of attitude control, since most spacecraft contain one or more spinning rotors to provide gyroscopic stability of a desired orientation or attitude of the vehicle. In this work, we follow the approach and adopt much of the notation presented in [13–16]. The transverse torque $\boldsymbol{\tau}$ acting on the flywheel is related to the rate of change of the wheel's angular momentum $\mathbf{L}$ with respect to an inertial reference frame $\mathcal{F}_I$ by

$$\frac{\mathrm{d}\mathbf{L}}{\mathrm{d}t} = \boldsymbol{\tau}. \tag{1}$$

The vehicle-flywheel system is modelled as a gyrostat; the rotor $\mathcal{R}$ (i.e. the flywheel) is pivoted within a body $\mathcal{B}$ that is formed by the vehicle to which the flywheel housing is rigidly connected. The vehicle-fixed coordinate frame $\mathcal{F}_B$ is spanned by the base vectors $\mathbf{b}_1$ (x-axis), $\mathbf{b}_2$ (y-axis) and $\mathbf{b}_3$ (z-axis) with an axes orientation according to ISO 8855 (Figure 1).

The inertia matrix $\mathbf{I}$ represents the total inertia of the vehicle, including the KERS. The principle moments of inertia of the rotor, on the other hand, are contained in $\mathbf{I}_r$. The rotational equation of motion (1) of $\mathcal{R}$ is transformed into the vehicle-fixed reference frame $\mathcal{F}_B$ by the well-known Euler equation

$$\mathbf{I}_r \frac{\mathrm{d}\boldsymbol{\omega}_r}{\mathrm{d}t} + \boldsymbol{\omega} \times \mathbf{I}_r \boldsymbol{\omega}_r = \boldsymbol{\tau}_r, \tag{2}$$

where we have to distinguish between the angular velocity $\boldsymbol{\omega}$ (which decomposes into roll, pitch and yaw rate) of $\mathcal{B}$ with respect to $\mathcal{F}_I$ and the angular velocity $\boldsymbol{\omega}_r$ of the flywheel. In order to have all quantities represented in the same frame, we use the reference frame $\mathcal{F}_B$ for the entire system $\mathcal{B} + \mathcal{R}$, which is fixed in the vehicle rather than in the flywheel. This is possible because the flywheel is symmetric about its spin axis and its inertia matrix remains constant even while the flywheel is spinning relative to $\mathcal{B}$. The total angular velocity $\boldsymbol{\omega}_r$ of

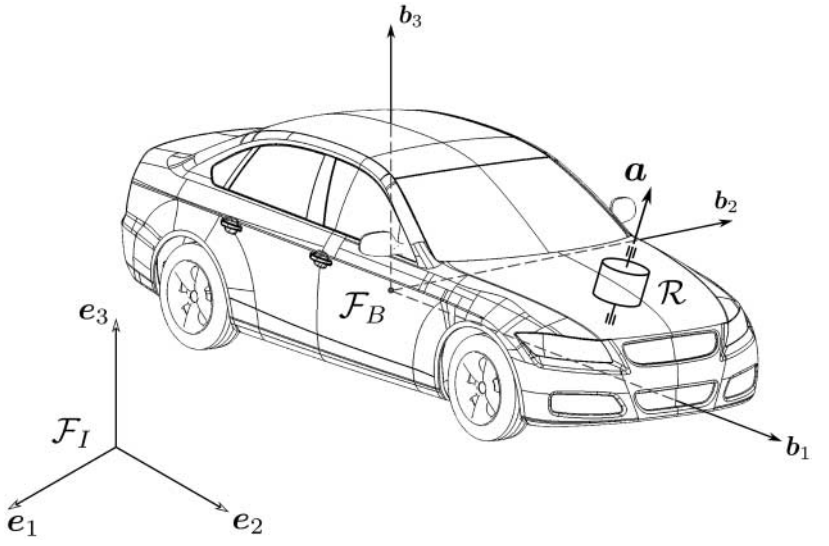

Figure 1. Schematic representation of the vehicle-KERS system (with the aid of the DrivAer car model [17]).

the flywheel consists of its relative spin ω_s and the angular velocity of the vehicle $\boldsymbol{\omega}$:

$$\boldsymbol{\omega}_r = \boldsymbol{\omega} + \omega_s \mathbf{a}, \tag{3}$$

with $\mathbf{a}$ being the unit vector representing the flywheel's spin axis. After substitution of Equation (3) and its derivative into Equation (2), the equation of motion becomes

$$\mathbf{I}_r(\dot{\boldsymbol{\omega}} + \dot{\omega}_s \mathbf{a}) + \boldsymbol{\omega} \times \mathbf{I}_r(\boldsymbol{\omega} + \omega_s \mathbf{a}) = \boldsymbol{\tau}_r. \tag{4}$$

The angular acceleration $\dot{\omega}_s$ of the flywheel can be found by taking the time derivative of the angular momentum of the flywheel relative to $\mathcal{F}_B$, which in the frame of reference $\mathcal{F}_R$ is given by

$$\mathbf{L}_s = I_s \omega_s \mathbf{a}; \tag{5}$$

the scalar quantity I_s represents the axial moment of inertia of the flywheel. In the inertial reference frame $\mathcal{F}_I$, however, the influence of the moving car on the flywheel must be taken into account, which is done by projecting the vehicle's angular velocity on the spin axis $\mathbf{a}$, and leads to

$$\mathbf{L}_a = I_s(\mathbf{a}^\mathsf{T}\boldsymbol{\omega} + \omega_s)\mathbf{a} \tag{6}$$

with $\mathbf{L}_a$ being the angular momentum of $\mathcal{R}$ about $\mathbf{a}$. The torque for spinning up or down the flywheel for storing or releasing kinetic energy, $\boldsymbol{\tau}_a$, causes the time rate of change of the flywheel's angular momentum:

$$\boldsymbol{\tau}_a = \frac{\mathrm{d}\mathbf{L}_a}{\mathrm{d}t} = I_s(\mathbf{a}^\mathsf{T}\dot{\boldsymbol{\omega}} + \dot{\omega}_s)\mathbf{a}. \tag{7}$$

By rearranging Equation (7), $\dot{\omega}_s$ can be expressed as

$$\dot{\omega}_s = \frac{\tau_a}{I_s} - \mathbf{a}^\mathsf{T}\dot{\boldsymbol{\omega}}. \tag{8}$$

Downloaded by [University of Otago] at 21:32 22 December 2014

Substituting Equation (8) in Equation (4) and simplifying gives

$$\boldsymbol{\tau}_r = \mathbf{I}_r \left[(\mathbb{1} - \mathbf{a}\mathbf{a}^{\mathsf{T}})\dot{\boldsymbol{\omega}} + \frac{\tau_a}{I_s}\mathbf{a} \right] + \boldsymbol{\omega} \times \mathbf{I}_r(\boldsymbol{\omega} + \omega_s \mathbf{a}) \tag{9}$$

with $\mathbb{1}$ representing the 3×3 unit matrix. The flywheel's moment of inertia tensor $\mathbf{I}_r$ is composed of transverse inertia I_t and axial inertia I_s and thus reads

$$\mathbf{I}_r = \begin{pmatrix} I_t & 0 & 0 \\ 0 & I_t & 0 \\ 0 & 0 & I_s \end{pmatrix}. \tag{10}$$

Rearranged and expressed in component notation, Equation (9) becomes

$$\begin{aligned} &\begin{pmatrix} I_t & 0 & 0 \\ 0 & I_t & 0 \\ 0 & 0 & I_s \end{pmatrix} \begin{pmatrix} 1-a_1^2 & -a_1a_2 & -a_1a_3 \\ -a_2a_1 & 1-a_2^2 & -a_2a_3 \\ -a_3a_1 & -a_3a_2 & 1-a_3^2 \end{pmatrix} \begin{pmatrix} \dot{\omega}_1 \\ \dot{\omega}_2 \\ \dot{\omega}_3 \end{pmatrix} \\ &+ \begin{pmatrix} 0 & -\omega_3 & \omega_2 \\ \omega_3 & 0 & -\omega_1 \\ -\omega_2 & \omega_1 & 0 \end{pmatrix} \begin{pmatrix} I_t & 0 & 0 \\ 0 & I_t & 0 \\ 0 & 0 & I_s \end{pmatrix} \left[\begin{pmatrix} \omega_1 \\ \omega_2 \\ \omega_3 \end{pmatrix} + \omega_s \begin{pmatrix} a_1 \\ a_2 \\ a_3 \end{pmatrix} \right] \\ &= \begin{pmatrix} \tau_{r_1} \\ \tau_{r_2} \\ \tau_{r_3} \end{pmatrix} + \frac{\tau_a}{I_s} \begin{pmatrix} I_t & 0 & 0 \\ 0 & I_t & 0 \\ 0 & 0 & I_s \end{pmatrix} \begin{pmatrix} a_1 \\ a_2 \\ a_3 \end{pmatrix} \end{aligned} \tag{11}$$

and represents a coupled system of three nonlinear, first-order differential equations, which in general can only be solved numerically.

The transverse torques $\boldsymbol{\tau}_r$ acting on the rotor will cause it to rotate about its centre of mass. The gyroscopic bearing loads can be easily derived from the transverse torques when the distance from the flywheel's centre of mass to the centreline of the radial bearings is known.

3. Integration of a KERS in a vehicle dynamics simulation

For the simulation of a passenger car's dynamic response to a flywheel-based KERS, the vehicle dynamics analysis program *veDYNA* (TESIS DYNAware GmbH, Munich, Germany [18]) is employed. *veDYNA* is based on a modelling concept that makes use of Jourdain's principle [19] and requires an MATLAB/Simulink (The MathWorks Inc., Natick, MA, USA) environment. The dynamical model consists of a chassis, axles, a steering mechanism, brakes, a drive train, an engine, a transmission and tyres. The chassis is modelled as a multi-body system comprising the rigid chassis body with six degrees of freedom (6 DOF). The axle bodies are guided kinematically to the chassis. The guidance with 1 DOF is described by kinematic tables. Compliances due to elastic deformation of the axle guidance are not considered. The wheel bodies are connected to the axle bodies using one rotational degree of freedom. A variable load corresponding to the mass of the KERS including the stator is fixed on the car body, thus considering the inertia of the KERS. The main differential equation systems use a semi-implicit Euler algorithm for integration that stays stable even at larger integration step sizes (in this work, a step size of 1 ms is used). The kernel functions are embedded in Simulink as C-coded s-functions, and the data flow between the components is established as Simulink signals and buses. The MATLAB/Simulink environment supports an open structure, which allows the implementation of the KERS as a Simulink model in the *veDYNA Vehicle System*

Downloaded by [University of Otago] at 21:32 22 December 2014

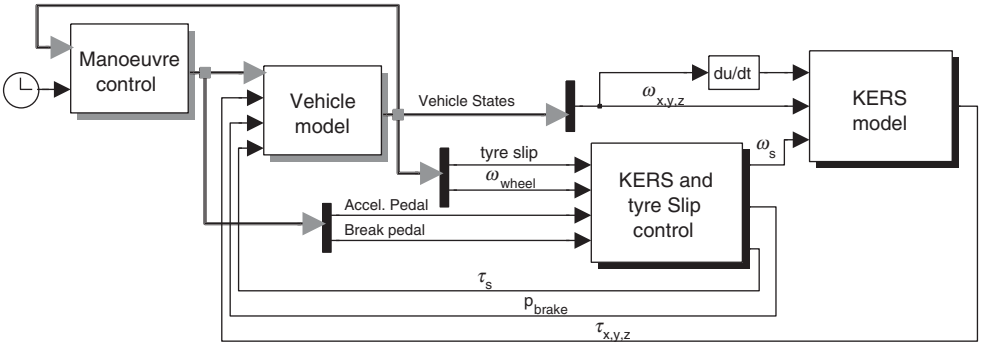

Figure 2. Block diagram of the reduced vehicle-KERS system.

Downloaded by [University of Otago] at 21:32 22 December 2014

subsystem. It processes the data provided by the vehicle dynamics simulation (roll, pitch and yaw rate, accelerator and brake pedal positions, angular velocities of the front wheels) and the flywheel's angular velocity in order to derive the gyroscopic reaction torques, the necessary brake pressure p_{brake} as well as the power transfer between KERS and vehicle (see block diagram in Figure 2).

The vehicle type chosen for the simulation is a limousine with the default vehicle parameters offered by *veDYNA*. Some geometry and simulation parameters are summarised in Table 1. A rear drive powertrain configuration with a manual transmission is chosen, where the manoeuvre controller comprises controls for clutch operation and gear shift as well as for the actuation of the accelerator, the brakes and the steering wheel. The engine torque is computed from a steady-state table characteristics describing the torque as a function of throttle angle and engine speed. The engine dynamics is accomplished by a first-order time delay. The integrated KERS Simulink model transfers power like a motor/generator unit to and from the front wheels, thus turning the vehicle into a hybrid car with regenerative braking.

In the original *veDYNA* model, the brake torque at each wheel is assumed to be produced by two brake pads that are pressed against a brake disc. The energy recovery strategy under regenerative braking is now as follows: if the required brake torque on the front axle does not exceed the maximum regenerative brake torque available, then only regenerative brake force is applied to the front wheels and a proper amount of frictional brake force on the rear axle is applied to maintain stability or avoid a wheel lock-up. If the available regenerative brake torque is exceeded by the braking demand, the hydraulic brake force supplies the excess braking power. The vehicle model is not equipped with an anti-lock braking system.

In the case of vehicle acceleration, the flywheel discharges its energy combined with the prime mover. The magnitude of the applied torque is governed by the driver's acceleration request and the vehicle velocity, since the speed of the flywheel has to be adapted to the front wheels' angular speed with the gear ratio of the CVT. The clutch operation of the KERS is controlled by the wheel slip, which results in a pulse width-modulated drive shaft torque. As tyre model for the slip control the semi-empirical *TMeasy* [20] is employed. The tyres roll on a flat road without surface waviness.

The simulation input, i.e. throttle position, brake pedal pressure and steering wheel angle, is either defined by a time-dependent table (open-loop manoeuvre) or by a driver model algorithm (closed-loop manoeuvre). In this work, the *basic driver without preview* algorithm was chosen, which follows a pre-described path with a target speed profile and does not utilise a preview control strategy.[21]

Table 1. Vehicle geometry and simulation parameters.

Vehicle length	4.32 m
Vehicle width	1.64 m
Vehicle height	1.16 m
Wheel base	2.57 m
Wheel track	1.40 m
Vehicle mass	1296 kg
Vehicle centre of gravity (CoG)[a]	$[-1.25, 0, 0.25]^{\intercal}$ m
Vehicle inertia at CoG	diag[305, 1520, 1750] kgm^2
Maximum engine torque (at 5000 rpm)	224 Nm
Maximum engine power (at 5100 rpm)	145 kW
Transmission gear ratio	First gear 3.830 Second gear 2.199 Third gear 1.401 Fourth gear 1.000 Fifth gear 0.810
Tyre size	205/60R13 88H
Sliding friction ratio[b]	0.95
Load degression for lateral force[b]	1.8
Maximum longitudinal force (at 3000 N load)	3180 N
Longitudinal slip gradient dF/ds	70,000 N
Maximum lateral force (at 3000 N load)	3180 N
Lateral slip gradient dF/ds	35,000 N
Tyre vertical stiffness	180,000 N/m
Suspension spring stiffness front/rear	17,098/27,183 N/m
Stabiliser stiffness front/rear	2610/197 Nm/$^\circ$
Damping rate compression front/rear[c]	1014/1064 Ns/m
Damping rate expansion front/rear[c]	2400/2950 Ns/m
Aerodynamic drag ($A \cdot c_d$)	0.8 m^2
KERS maximum power	60 kW
Flywheel inertia	$I_s = 0.026$ kgm^2
Maximum flywheel speed	$n_{\max} = 64,500$ rpm
Minimum flywheel speed	$n_{\min} = 15,000$ rpm

[a]CoG measured from centre of front axle.
[b]Parameters of the *veDYNA light* model.
[c]Mean values due to nonlinear characteristics.

4. Investigation of some selected driving manoeuvres

In this section, the dynamic response of the vehicle to the flywheel-based KERS is investigated by simulations of some standardised and non-standardised driving manoeuvres. The use of the KERS is limited to transient phases, that is, to acceleration and braking, while the propulsion during constant speed phases is solely accomplished by the combustion engine.

The KERS is located at the centre of gravity of the car and the flywheel's axis of rotation is vertically aligned ($\mathbf{a} = \mathbf{b}_3$) in order to minimise gyroscopic torques caused by cornering and turning. We have adopted the *Flybrid Systems* specifications [4] for the Formula 1 KERS in our simulations (Table 1). KERSs of this type are recently in use not only in motorsports but increasingly in mass-produced road vehicles. This system's high-speed flywheel, which is supported by mechanical bearings, is built much smaller and lighter than has previously been possible, which allows the avoidance of softly suspended or gimballed mounting systems. In this work, the flywheel housing is assumed to be mounted rigidly to the chassis body, thus establishing a direct coupling with the vehicle.

4.1. *Straight-line driving*

In the straight-line driving manoeuvre, the car accelerates as fast as possible until a time limit of 20 s is reached. The car is then allowed to settle and the brake is activated with 25% of

Downloaded by [University of Otago] at 21:32 22 December 2014

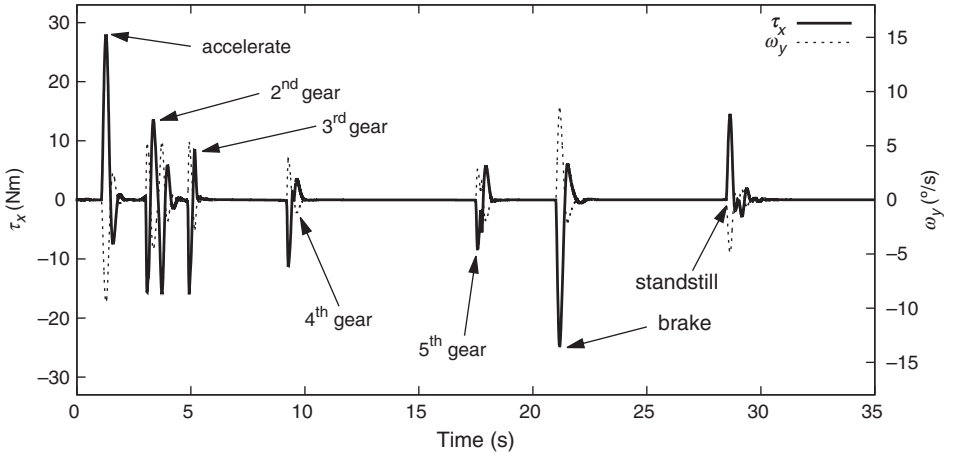

Figure 3. Straight-line driving manoeuvre with fixed steering wheel and fully charged KERS: torque τ_x and pitch rate ω_y.

the available braking force. This percentage is chosen in order to prevent the wheels from locking when the KERS is charged during the regenerative braking mode. This manoeuvre serves for the investigation of the gyroscopic torques induced by pitch oscillations caused by pulling away, gear shifting, braking and vehicle standstill.

4.1.1. *Straight-line driving with fixed steering and fully charged KERS*

At first, the flywheel remains fully charged and rotates with 64, 500 revolutions per minute during the entire manoeuvre. Energy recuperation during braking and KERS-induced acceleration boosts are thus disabled. The resulting torque τ_x caused by the pitch rate ω_y can be seen in Figure 3. The maximum torque (represented by the full line in the figure) of approximately 28 Nm is reached while the car starts at full throttle. This torque acts clockwise in x-direction and thus increases the vertical tire load on the right-hand side of the vehicle, which causes the vehicle to drift slightly to the right when the steering wheel is fixed in neutral position. After about 3 s the driver model shifts into the second gear and the pitch rate (represented by the dotted line in Figure 3) starts to oscillate and causes the torque τ_x to oscillate as well for more than 1 s. Shifting into the higher gears leads to shorter oscillations and successively less gyroscopic torque. The longitudinal load transfer incidental to the braking (at about second 22 in Figure 3) causes the car to pitch forward, which increases the tire load on the left-hand side due to the resulting gyroscopic torque. Thus, the car starts to drift slightly to the left as long as no counter-steering torque is applied.

The gyroscopic torque caused by the pitch motion of the vehicle produces the slight roll rate depicted in Figure 4(a). The resulting gyroscopic torque in y-direction, however, is about two orders of magnitude smaller than τ_x. The small yaw rate illustrated in Figure 4(b) stems from the weight shift caused by τ_x; no torque can be observed in z-direction due to the parallel alignment of the flywheel's axis.

4.1.2. *Straight-line driving with fixed steering and charging/discharging KERS*

As a next step, the charging and discharging of the KERS is included in the same simulation, which ought to lead to an additional torque in z-direction. This torque occurs when power

Downloaded by [University of Otago] at 21:32 22 December 2014

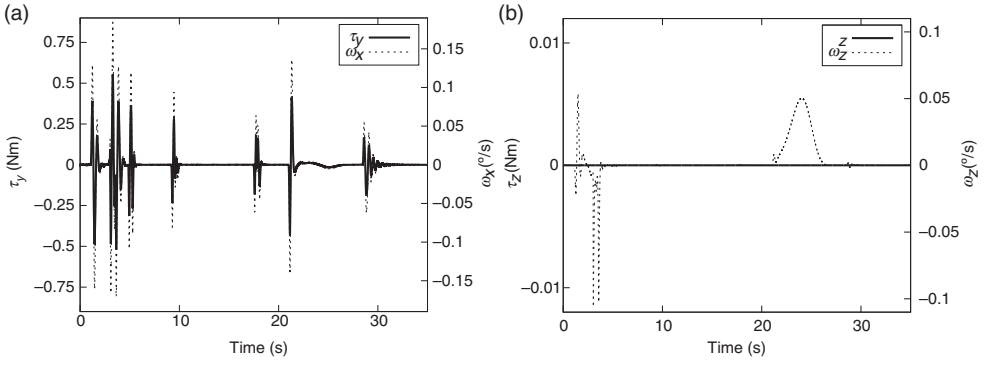

Figure 4. Straight-line driving manoeuvre with fixed steering wheel and fully charged KERS: (a) torque τ_y and roll rate ω_x, and (b) torque τ_z and yaw rate ω_z.

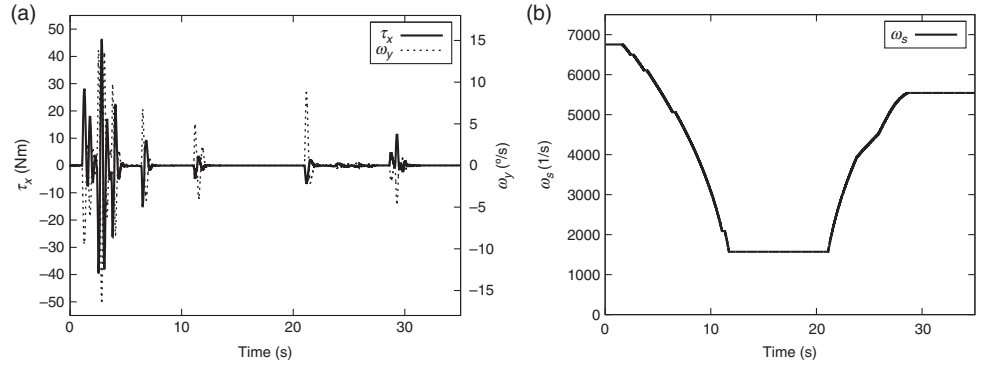

Figure 5. Straight-line driving manoeuvre with fixed steering wheel and discharging/charging KERS: (a) torque τ_x and pitch rate ω_y, and (b) angular frequency ω_s of discharging/charging KERS.

is extracted from the flywheel and fed to the front wheels, or vice versa during regenerative braking. The manoeuvre is once again performed with the steering wheel kept fixed in neutral position. Due to the boost provided by the KERS, the vehicle accelerates faster and the simulation switches to the top gear after 11 s (Figure 5(a)). The torque distribution is similar to Figure 3 in the acceleration phase, apart from the faster succession of gear changes resulting in higher peak torques. The angular velocity profile ω_s of the flywheel is illustrated in Figure 5(b). The system provides power for approximately 11 s until the minimum rotational speed of 15,000 revolutions per minute is reached. Gear shifting can be recognised by horizontal shifts in the declining branch of the angular velocity curve.

Figure 6(b) shows the torque τ_z, which is extracted from or fed to the flywheel. The hyperbolic increase during the acceleration phase corresponds to the decrease in angular velocity due to power extraction from the KERS (Figure 5(b)). During gear shifting the torque flow is interrupted by the clutch, as depicted by the vertical discontinuities. When braking is applied, the flywheel is at its minimum angular speed and acts now as the primary brake. The brake pressure at the front wheels is reduced accordingly by the amount of the regenerative braking force. The control algorithm providing a proper KERS clutch engagement and disengagement and the continuous change of ratio between flywheel and road-wheel speed prevents wheel spin under acceleration and wheel lock-up during regenerative braking. The fast control loop causes the black areas in the τ_z graph displayed in Figure 6(b) during full throttle start and before standstill.

Downloaded by [University of Otago] at 21:32 22 December 2014

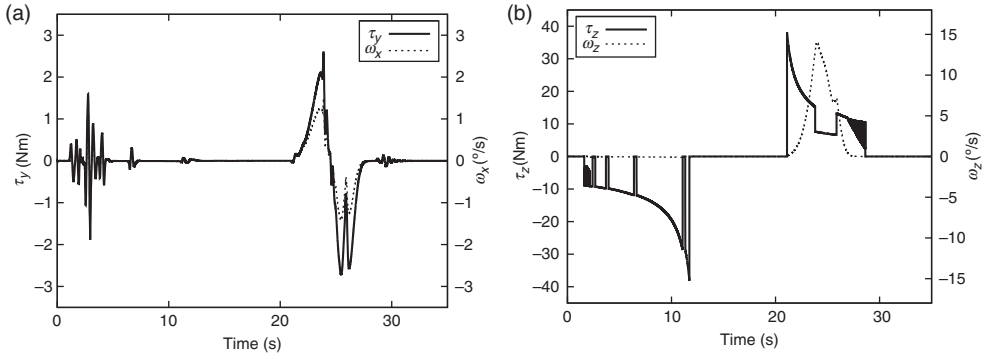

Figure 6. Straight-line driving manoeuvre with fixed steering wheel and discharging/charging KERS: (a) torque τ_y and roll rate ω_x, and (b) torque τ_z and yaw rate ω_z.

The roll rate ω_x introduced by the gyroscopic torque τ_x produces a gyroscopic torque in y-direction (Figure 6(a)), which leads to a noticeable imbalance in the wheel load on the left and right front wheels. The left wheel carries less dynamic tyre load than the right one and locks up for 3 s during braking. In addition, the vehicle tends to yaw due to the charging torque of the flywheel, τ_z. The combination of lateral and longitudinal forces with the limitation of the friction ellipse results in a saturation of tyre forces, effectively causing a noticeable yaw rate in the braking phase (Figure 6(b)).

While the left wheel locks only half of the kinetic energy is recuperated, which leads to the distinctive drop in the τ_z curve in Figure 6(b). The reduced charging capability of the KERS during the wheel lock is also recognisable in the ω_s profile in Figure 5(b)).

4.1.3. *Controlled straight-line driving with charging/discharging KERS*

The open-loop straight-line driving manoeuvres are supplemented by a closed-loop controlled manoeuvre with a driver model that follows a straight-line course in the presence of flywheel-induced yaw and roll torque. The driver model, which is based on a fully nonlinear position control law designed for set-point trajectory tracking, has the sole task to counteract the influence of the gyroscopic torque. Within the same simulation scenario as before the car accelerates as fast as possible from rest and decelerates after 20 s with 25% of the available braking force until standstill is reached. The pitch rate ω_y and corresponding gyroscopic torque τ_x are almost identical to those derived in the fixed steering wheel manoeuvre, as illustrated in Figure 7(a). This result is to be expected since a moderate deviation from straight-line driving should not noticeably influence the longitudinal dynamics.

The steering input of the driver model has much more influence on the yaw and roll rate of the vehicle. The roll rate ω_x increases in the acceleration phase and vanishes almost entirely during braking (Figure 8(a)). Thus, the gyroscopic pitch torque τ_y is negligible during the vehicle's deceleration phase. The yaw rate ω_z, on the other hand, is reduced by an order of magnitude over the entire range of simulation. As a consequence of this, the tyre loads are much better balanced and the wheels do not lock up during regenerative braking. The τ_z curve proceeds continuously during both charging and discharging of the KERS, as depicted in Figure 8(b). This leads to a higher state of charge of the system; the flywheel's final angular velocity ω_s is about 5000 revolutions per minute higher than in the fixed steering wheel case (Figure 7(b)).

With the stipulation of a maximum steering wheel rate of 720°/s of *veDYNA*'s proportional-integral controller, the closed-loop steering wheel angle δ_{sw} history reveals only

Downloaded by [University of Otago] at 21:32 22 December 2014

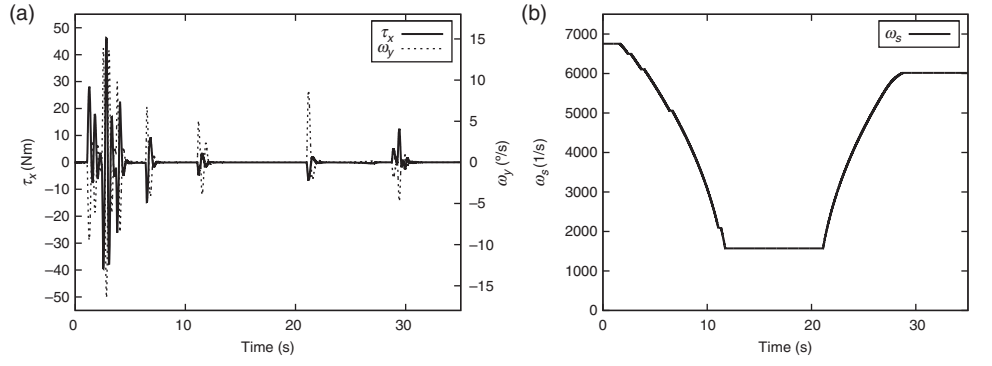

Figure 7. Controlled straight-line driving manoeuvre with discharging/charging KERS: (a) torque τ_x and pitch rate ω_y, and (b) angular frequency ω_s of discharging/charging KERS.

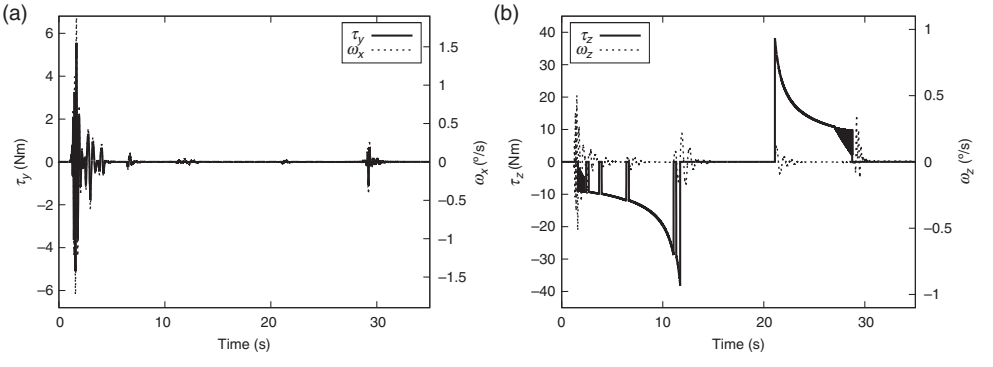

Figure 8. Controlled straight-line driving manoeuvre with discharging/charging KERS: (a) torque τ_y and roll rate ω_x, and (b) torque τ_z and yaw rate ω_z.

small steering corrections, except when the vehicle is pulling away from rest (Figure 9). During the gear-shifting phase and while braking, the steering wheel angles remain well below 3°, which would be hardly perceptible to a human driver. In Figure 9, the torque τ_x responsible for wheel load disparities is superimposed to δ_{sw}.

Both τ_x and τ_y are higher in magnitude during the acceleration phase when the KERS is discharging. This is due to the additional acceleration boost provided by the system, which leads to a considerable improvement of the vehicle's performance. Under the idealised assumption that 100% of the stored power can be returned to the wheels, the acceleration from 0 to 100 km/h takes 2.4 s less than without the extra power on the front axle, and the top speed after 20 s increases from 160 to 180 km/h (Figure 10).

4.2. *ISO 3888 lane change test*

A lane change manoeuvre with fully charged KERS is simulated in order to introduce lateral dynamics in the investigations. The ISO 3888 specification for a double lane change manoeuvre, originally known as the 'moose test', is widely used to evaluate the handling and safety of vehicles and their key components. Based on three cone lanes with a total length of 61 m a double lane change is defined, which must be completed with maximum speed. It simulates a situation where an obstacle suddenly appears in front of the car, which forces the driver to swerve onto the opposite side of the road and then back to the travel direction side in order

Downloaded by [University of Otago] at 21:32 22 December 2014

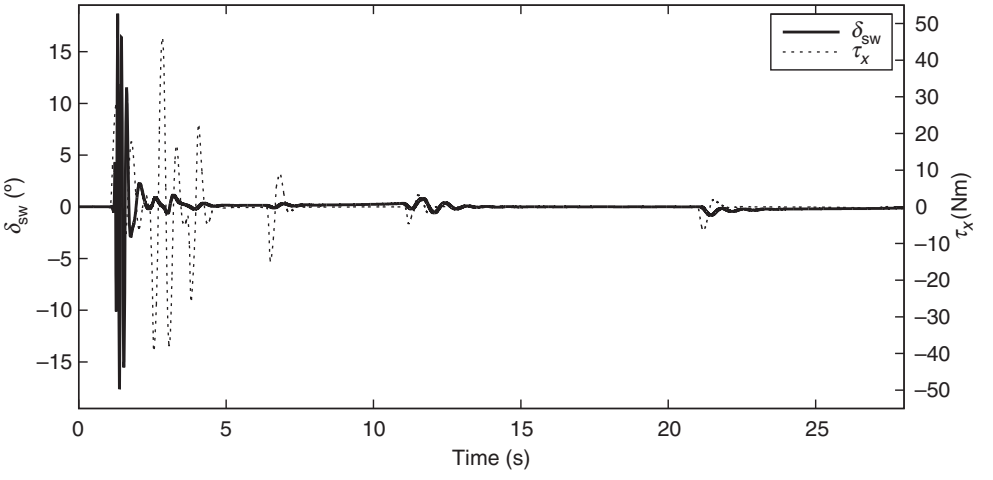

Figure 9. Controlled straight-line driving manoeuvre with discharging/charging KERS: steering wheel angle δ_{sw}.

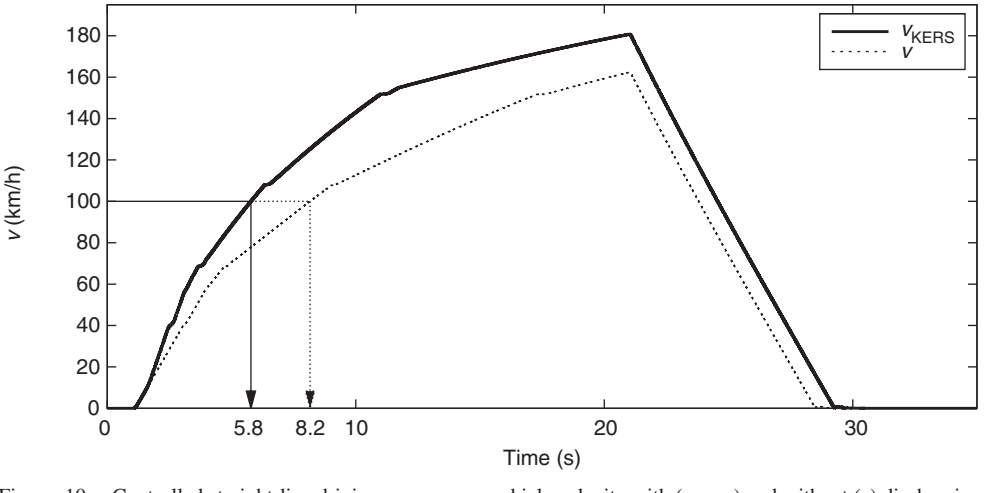

Figure 10. Controlled straight-line driving manoeuvre: vehicle velocity with (v_{KERS}) and without (v) discharging KERS.

to avoid an accident. The test consists of an entry lane (12 m), a side lane (11 m) and an exit lane (12 m). The width of the exit lane is constantly 3 m, while the width of the entry and side lane are dependent on the width of the vehicle. The lateral offset between entry and side lane is 3.5 m and the longitudinal offset 13.5 m. The exit lane has the same lateral offset but a slightly shorter longitudinal one (12.5 m). The speed of entry is 80 km/h and the throttle position is held steady over the test course. The test is passed if no cones are overturned.

In Figures 11 and 12, the lane changes take place between second 27 and second 33. The roll rate caused by the lane change (first turn to the left-hand side) induces a gyroscopic torque in y-direction of less than 10 Nm (Figure 11(b)). This torque causes a slight shift of the tire loads between front and rear wheels, which turns out to be negligible in terms of driveability. The highest torques occur in x-direction due to the pitch rate caused by acceleration and braking of the car as well as due to gear shifting, as depicted in Figure 11(a).

Downloaded by [University of Otago] at 21:32 22 December 2014

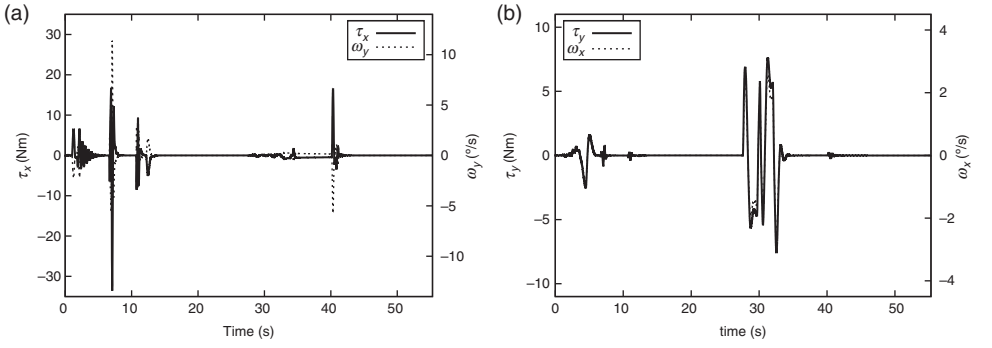

Figure 11. VDA lane change test with fully charged KERS: (a) torque τ_x and pitch rate ω_y, and (b) torque τ_y and roll rate ω_x.

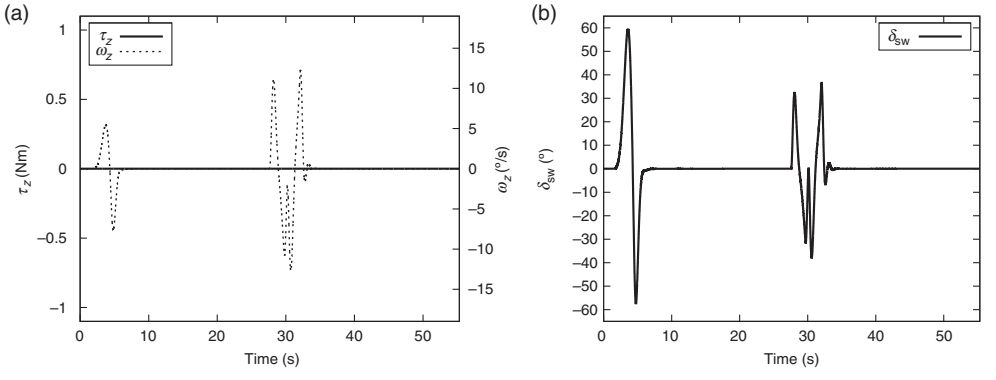

Figure 12. VDA lane change test with fully charged KERS: (a) torque τ_z and yaw rate ω_z, and (b) steering wheel angle δ_{sw}.

4.3. *ISO 7975 braking in a turn*

Another open-loop test procedure, the ISO 7975 braking in a turn manoeuvre, is simulated in order to examine the effect of braking on course holding and directional behaviour of the vehicle. Specifically, the procedure determines how the steady-state circular response of the vehicle is altered by the braking action with fully charged KERS as well as with regenerative braking. In this simulation the car drives along a circular path and accelerates up to a predefined velocity. After a few seconds of constant speed, the brakes are applied according to the test standard and the vehicle is brought to rest. The curve radius for this simulation is chosen to be 40 m, and the maximum speed of the car is 51 km/h.

The yaw rate ω_z increases with vehicle speed, as illustrated in Figure 13. The small peak that occurs before the vehicle holds its speed is caused by the driver control model that applies the brake when approaching the final velocity. This braking action causes a pitch rate that becomes responsible for the highest torque peak (τ_x) during the entire manoeuvre (Figure 14). All the torques vanish when the vehicle is driving at constant speed along the curve and re-emerge at the start and the end of the deceleration phase. In both Figures 14 and 15, the torques in x- and y-direction are compared for the manoeuvre performed with fully charged (top) and recharging KERS (bottom), respectively. The amplitude ratio of the gyroscopic torques is proportional to the corresponding angular frequency of the flywheel.

Downloaded by [University of Otago] at 21:32 22 December 2014

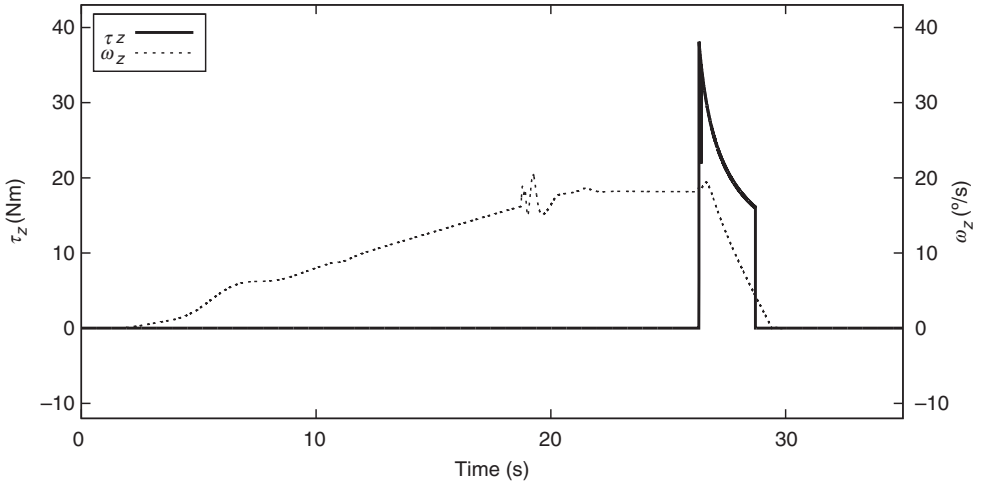

Figure 13. Braking in a turn with charging KERS: torque τ_z and yaw rate ω_z.

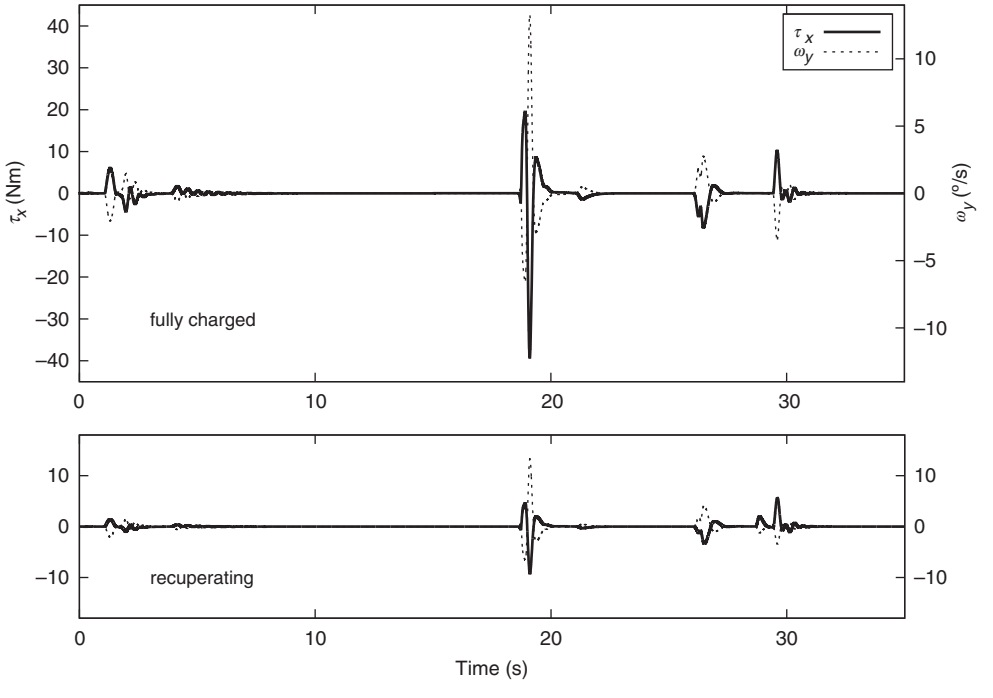

Figure 14. Braking in a turn: torque τ_x and pitch rate ω_y.

4.4. *Speed bump*

In all analyses so far the pitch rate proves to be the major cause for appreciable gyroscopic torque. Driving over speed bumps usually induces large amplitude pitch oscillations, which in turn could cause gyroscopic reactions. For the simulation of such a manoeuvre, a ramp is defined in the *veDYNA* standard road module in order to mimic a speed bump, which can often be seen in residential streets or reduced traffic areas. The speed bump (width 500 mm

Downloaded by [University of Otago] at 21:32 22 December 2014

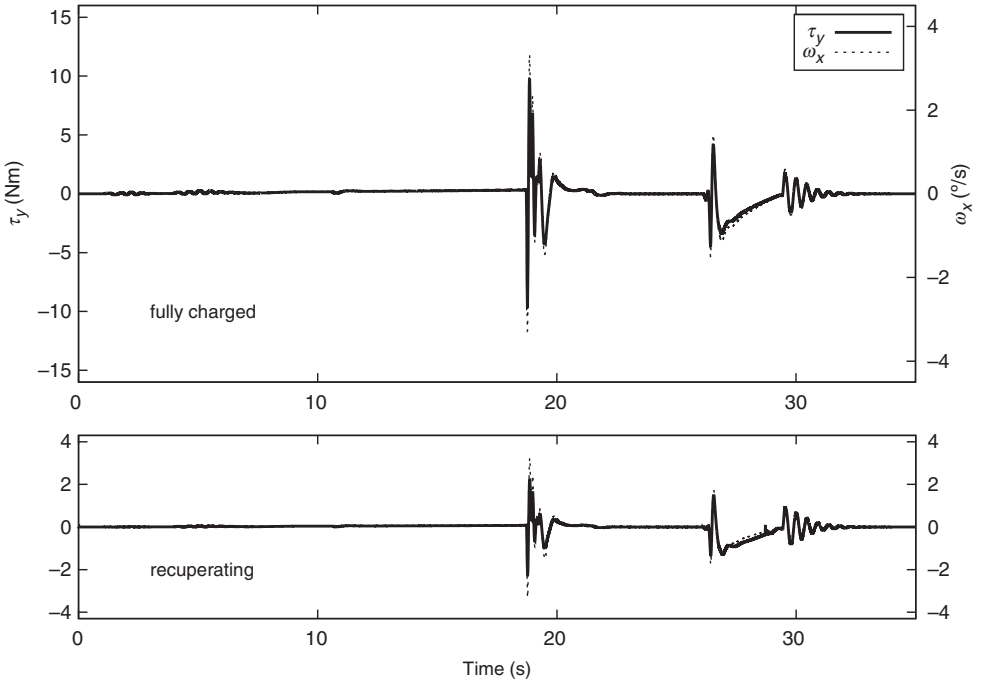

Figure 15. Braking in a turn: torque τ_y and roll rate ω_x.

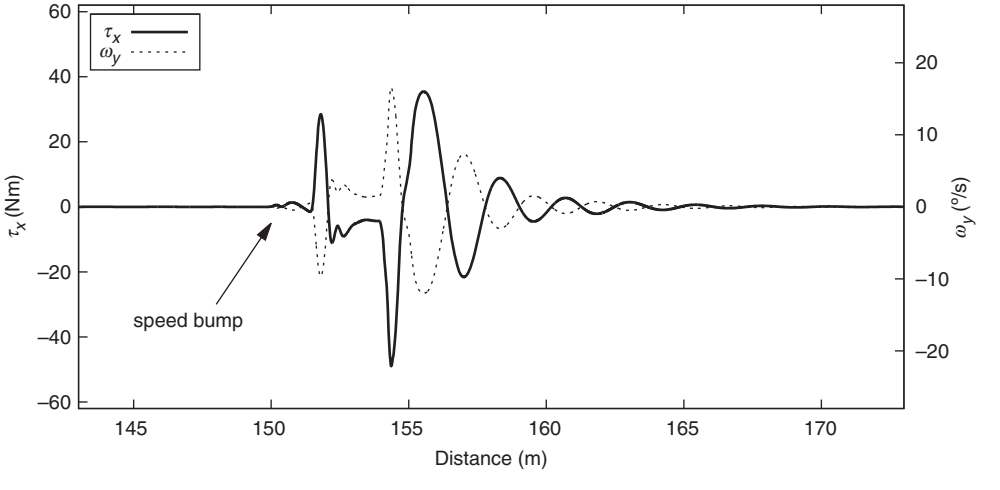

Figure 16. Traversing a speed bump at 20 km/h: torque τ_x and pitch rate ω_y.

and height 70 mm) is placed 150 m after the start position and the vehicle is driven over the bump at the relatively slow speed of 20 km/h. Figure 16 depicts the decaying oscillation of the pitch rate ω_y after the car has passed the speed bump. The thus produced gyroscopic torque (τ_x) reaches a magnitude of almost 50 Nm, which is comparable with the torque caused by judder when the car is pulling away under KERS acceleration boost (Figures 5(a) and 7(a)).

Further simulations with a traversal of the speed bump at 40 km/h revealed that the highest gyroscopic torques remain below 60 Nm.

Downloaded by [University of Otago] at 21:32 22 December 2014

5. Summary and conclusion

The dynamic response of a passenger car to a flywheel-based KERS is investigated by computer simulations of standardised and non-standardised driving manoeuvres that cover a representative range of driving situations. To this end a coupled system of nonlinear differential equations is derived, which relates the vehicle's roll, pitch and yaw rate with the transverse torque acting on the flywheel. These equations are implemented in Simulink and integrated as an extension of the commercial vehicle dynamics simulation program *veDYNA* in order to determine the reaction torques acting on the vehicle. Four different driving manoeuvres that comprise longitudinal as well as lateral vehicle dynamics are conducted and the ensuing reaction torques and angular velocities of the vehicle are presented and discussed.

In both longitudinal and lateral manoeuvres, the roll torque caused by the vehicle's pitch rate dominates. Within the chosen system parameters its magnitude stays well below 60 Nm in all simulations even when the KERS is fully loaded. The roll torque causes a roll rate, which, on the other hand, induces a pitch torque that is smaller by an order of magnitude due to the vehicle's inertia. As a consequence of this pitch torque a load transfer takes place, which leads to a tyre load imbalance that causes the vehicle to yaw slightly. Barring the case of fixed steering wheel, which is of rather academic interest, this effect is easily controllable.

When subjected to bump riding events the gyroscopic torques do not exceed 60 Nm even at intermediate speed. Lateral dynamics manoeuvres like the 'moose test' or braking in a curve additionally induce pitch torques of less than 15 Nm.

In conclusion, although the flywheel is rigidly mounted in the passenger car there is only a subtle influence on the vehicle dynamics due to the induced gyroscopic torques, which can be considered insignificant in standard driving situations.

Downloaded by [University of Otago] at 21:32 22 December 2014

Funding

This work was supported by the Austrian Research Promotion Agency [grant number FFG 825553 NE-IF]: *PowerKERS–Flywheel als Energiespeicher in Hybrid- und Elektrofahrzeugen für den Individualverkehr*.

References

[1] Post R. A new look at an old idea – the electromechanical battery. Sci Technol Rev. 1996 April:12–19.
[2] Schilke NA, Dehart AO, Hewko LO, Matthews CC, Pozniak DJ, Rohde SM. The design of an engine-flywheel hybrid drive system for a passenger car. SAE Technical Paper 841306. Warrendale (PA): SAE International; 1984.
[3] Hansen JGR, O'Kain DU. An assessment of flywheel high power energy storage technology for hybrid vehicles. Report ORNL/TM-2010/280. Oak Ridge National Laboratory; 2011.
[4] Cross D, Brockbank C. Mechanical hybrid system comprising a flywheel and CVT for motorsport and mainstream automotive applications. SAE Technical Paper 2009-01-1312. Warrendale (PA): SAE International; 2009.
[5] Boretti A. Improvements of vehicle fuel economy using mechanical regenerative braking. SAE Technical Paper 2010-01-1683. Warrendale (PA): SAE International; 2010.
[6] Brockbank C, Greenwood C. Fuel economy benefits of a flywheel & CVT based mechanical hybrid for city bus and commercial vehicle applications. SAE Int J Commer Veh. 2010;2(2):115–122.
[7] Moro D, Cavina N, Trivić I, Ravaglioli V. Guidelines for integration of kinetic energy recovery system (KERS) based on mechanical flywheel in an automotive vehicle. SAE Technical Paper 2010-01-1448. Warrendale (PA): SAE International; 2010.
[8] Boretti A. Modeling of engine and vehicle for a compact car with a flywheel based kinetic energy recovery systems and a high efficiency small diesel engine. SAE Technical Paper 2010-01-2184. Warrendale (PA): SAE International; 2010.
[9] Rauh J, Ammon D. System dynamics of electrified vehicles: some facts, thoughts, and challenges. Veh Syst Dyn. 2011;49(7):1005–1020.
[10] Boretti A. Braking for 2014 F1 cars. SAE Technical Paper 2012-01-1802. Warrendale (PA): SAE International; 2012.

[11] Metz L. Potential for passenger car energy recovery through the use of kinetic energy recovery systems (KERS). SAE Technical Paper 2013-01-0407. Warrendale (PA): SAE International; 2013.
[12] Yoshihiro S, Junhoi H, Masahiko A, Lin S, Takahata R, Mukaide N. Study on rollover prevention of heavy-duty vehicles by using flywheel energy storage systems. Proceedings of the FISITA 2012 World Automotive Congress, Lecture Notes in Electrical Engineering. Vol. 197; 2013. p. 693–701.
[13] Hughes PC. Spacecraft attitude dynamics. New York: John Wiley & Sons; 1986.
[14] Hall CD, Rand RH. Spinup dynamics of axial dual-spin spacecraft. J Guid Control Dyn. 1994;17(1):30–37.
[15] Hall CD. Spinup dynamics of gyrostats. J Guid Control Dyn. 1995;18(5):1177–1183.
[16] Pressl MC. Internal torques and forces in gyrostats with magnetically suspended rotors [M.S. thesis]. Blacksburg (VA): Virginia Polytechnic Institute and State University; 2003.
[17] Heft AI, Idinger T, Adams NA. Introduction of a new realistic generic car model for aerodynamic investigations. SAE Technical Paper 2012-01-0168. Warrendale (PA): SAE International; 2012.
[18] Chucholowski C, Vögel M, Stryk O, Wolter T-M. Real time simulation and online control for virtual test drives of cars. In: Bungartz H-J, Durst F, Zenger C, editor. High Performance Scientific and Engineering Computing, Vol. 8 (Lecture Notes in Computational Science and Engineering). Berlin: Springer; 1999, p. 157–166.
[19] Rill G. Road vehicle dynamics: fundamentals and modeling (Ground Vehicle Engineering Series). Boca Raton, FL: CRC Press Inc.; 2011.
[20] Hirschberg W, Rill G, Weinfurter H. Tire model TMeasy. Veh Syst Dyn. 2007;45(1):101–119.
[21] Irmscher M, Ehmann M. Driver classification using ve-DYNA advanced driver. SAE Technical Paper 2004-01-0451. Warrendale (PA): SAE International; 2004.

Downloaded by [University of Otago] at 21:32 22 December 2014